IEEE Access
Multidisciplinary | Rapid Review | Open Access Journal

Received June 2, 2021, accepted June 14, 2021, date of publication June 17, 2021, date of current version June 28, 2021.

Digital Object Identifier 10.1109/ACCESS.2021.3090104

Robust Beamforming Based on Weighted Vector Norm Regularization

XIAOYING REN[1], YINGMIN WANG[1], (Member, IEEE), LICHEN ZHANG[2], AND QI WANG[1]
[1]School of Marine Science and Technology, Northwestern Polytechnical University, Xi'an 710072, China
[2]System Engineering Research Institute, Beijing 100094, China

Corresponding author: Yingmin Wang (ywang@nwpu.edu.cn)

This work was supported by the National Natural Science Foundation of China under Grant 51879221.

ABSTRACT Steering vector mismatch rapidly degrades the performance of the minimum variance distortionless response beamformer. To solve this problem, a robust beamforming method based on weighted vector norm regularization is proposed. First, the factors affecting the robustness of the beamformer are analyzed. Second, by introducing the weighted vector norm, an optimization problem is constructed to increase the robustness of the beamformer. Furthermore, the regularization coefficient is provided to achieve a balance between the output power and the robustness of the beamformer. Meanwhile, a method of finding the appropriate regularization coefficient is provided. Then, simulations of an irregular arc array are carried out, showing that the proposed method is robust to the snapshot number. Finally, the results and data analysis indicate the effectiveness of the proposed method.

INDEX TERMS Beamforming, robustness, regularization, spatial resolution, weighted vector norm.

I. INTRODUCTION

As an array signal processing method, beamforming has been widely used in many fields, such as communication [1], radar [2], sonar [3], imaging [4], mapping [5], and remote sensing [6]. In the conventional beamforming (CBF) method, the signals from different directions are delayed differently, and then all the delayed signals are summed up such that the signals from different directions obtain different magnifications. The beam pattern of CBF is unaffected by the snapshot number because the weighted vector calculated by the CBF method is determined by the assumed steering vector and the number of array elements. However, the interference suppression ability of CBF is limited. Therefore, the output signal-to-interference-plus-noise ratio (SINR) of CBF can hardly meet the design requirements when the received data contains interference. To improve the output SINR of the beamformer, Capon [7] proposed the minimum variance distortionless response (MVDR) beamforming method. The MVDR beamformer can ensure that the output of the desired signal is not distorted and minimize the output power of interference plus noise. The MVDR beamformer can achieve optimal performance when the snapshot number is sufficient and the actual steering vector is known. Unfortunately, insufficient snapshot number and steering vector mismatch are often encountered in practical application scenarios. When the snapshot number is insufficient, the sidelobe of MVDR will increase because the estimated covariance matrix is inaccurate [8]. Meanwhile, when a mismatch in the steering vector exists, the signal self-cancellation phenomenon will occur because the signal is mistakenly suppressed as interference [9]. These two phenomena will lead to a sharp decrease in the output SINR and a serious degradation in the performance of the MVDR beamformer.

To improve the robustness of the beamformer, many robust beamforming methods have emerged through studies on array signal processing. These methods are mainly divided into diagonal loading methods [10], [11], eigenspace-based methods [12], [13], and sparse-constraint-based methods. An inappropriate diagonal loading factor will cause a sharp decline in the performance of the beamformer. Many methods have been proposed to determine the optimal diagonal loading factor. These methods obtain the optimal diagonal loading factor by combining matrix theory with experimental method [14], estimating the signal-to-noise ratio (SNR) of the sample covariance matrix [15], or combining denoising pretreatment with truncated least mean square error theory [16]. Diagonal loading methods can improve the robustness of the beamformer to a certain extent. Unfortunately, the optimal diagonal loading factor is difficult to determine

The associate editor coordinating the review of this manuscript and approving it for publication was Guolong Cui.

due to the uncertainty error of the steering vector in actual scenarios. Eigenspace-based methods can improve the robustness of the beamformer by taking advantage of the eigenspace characteristics of the received data. According to the minimum sensitivity principle, the optimal projection of the weighted vector can be obtained by using the sensitivity function in the enhanced eigenspace beamformer [17]. By combining the approximate expression of signal subspace projection and the two-stage beamformer structure, the beamformer can eliminate the subspace projection operation and the element number estimation [18]. However, these methods can hardly realize spatial filtering when the SNR is not high enough or the number of the desired signal plus interferences is extremely high [12]. With the wide application of sparse representation in statistical signal processing and parameter estimation [19]–[22], some sparse-constraint-based beamforming methods have emerged [23], [24]. Given the sparse distribution of interferences in the sidelobe region, the array response in the sidelobe region is sparsely constrained in these methods. These sparse-constraint-based beamforming methods can reduce the sidelobe level of the beam pattern and improve the robustness of the beamformer. Notwithstanding, these methods require a priori knowledge of the direction of arrival (DOA) of interferences, which is often difficult to achieve in practical applications. In addition, a reconstruction-based beamformer can reduce the performance degradation caused by sensor gain and phase uncertainty [25]. A beamformer based on support vector machine can improve the robustness of the beamforming algorithm without reducing the spatial resolution, but the main lobe width of this method must be set reasonably according to experience [26]. A method improves the performance by calibrating the position, gain, and phase of the array elements [27]. The various beamforming methods mentioned above improve the robustness and performance of the beamformer in different ways. However, the implementation process of these methods is complex or they need prior knowledge which is difficult to obtain in actual scenarios.

To find a robust beamforming method that is simple and easy to implement, the weighted vector norm regularization (WVNR) beamforming method is proposed. To directly control the robustness of the beamformer, the factors affecting the robustness are analyzed in this paper. The weighted vector norm directly affects the robustness of the beamformer. In the proposed WVNR method, the weighted vector norm is added to the objective function of the MVDR model as a regularization term. The regularization coefficient controls how much weight is assigned to the minimization of the weighted vector norm relative to the minimization of the output power. By fitting the cubic spline curve and calculating the maximum curvature, the optimal regularization coefficient can be derived. Computer simulations of an irregular arc array are carried out, and the results show that the WVNR method can effectively improve the robustness of the beamformer to the snapshot number and steering vector mismatch.

II. BACKGROUND

Assuming that the elements of an arbitrary array are all omnidirectional sensors, the number of elements is M, the number of narrowband plane waves received by the array is $J+1$, and the number of interferences is J. After the digital sampling of the analog waves, the time domain model of the signals received by the array at time k can be expressed as

$$\boldsymbol{x}(k) = \boldsymbol{a}(\theta_s)\, s_s(k) + \sum_{j=1}^{J} \boldsymbol{a}\left(\theta_j\right) s_j(k) + \boldsymbol{n}(k), \tag{1}$$

where k is the index of the temporal samples, and $j = 1, 2, \cdots, J$ is the index of interferences. $s_s(k)$, $\boldsymbol{a}(\theta_s)$, and θ_s are the waveform, the steering vector, and the DOA of the desired signal, respectively. $s_j(k)$, $\boldsymbol{a}\left(\theta_j\right)$, and θ_j represent the waveform, the steering vector, and the DOA of interference, respectively. $\boldsymbol{n}(k)$ is the spatial Gaussian white noise vector.

The output of the narrowband beamformer is

$$\boldsymbol{y}(k) = \boldsymbol{w}^H \boldsymbol{x}(k), \tag{2}$$

where $\boldsymbol{w}$ is the weighted vector, and $\boldsymbol{w} = [w_1, w_2, \cdots, w_M]^T$. Here, $(\cdot)^T$ denotes transpose, and $(\cdot)^H$ denotes conjugate transpose.

The output SINR of the beamformer is

$$SINR = \frac{\sigma_{ys}^2}{\sigma_{yj}^2 + \sigma_{yn}^2} = \frac{\boldsymbol{w}^H \boldsymbol{R}_s \boldsymbol{w}}{\boldsymbol{w}^H \boldsymbol{R}_j \boldsymbol{w} + \boldsymbol{w}^H \boldsymbol{R}_n \boldsymbol{w}}, \tag{3}$$

where σ_{ys}^2, σ_{yj}^2, and σ_{yn}^2 are the output powers of the desired signal, interference, and noise, respectively; $\boldsymbol{R}_s$, $\boldsymbol{R}_j$, and $\boldsymbol{R}_n$ are the covariance matrices of the desired signal, interference, and noise, respectively.

For the CBF algorithm, the weighted vector is

$$\boldsymbol{w}_{CBF} = \boldsymbol{a}(\theta_0)/M, \tag{4}$$

where $\boldsymbol{a}(\theta_0)$ is the assumed steering vector, and θ_0 is the angle of the assumed steering vector.

To improve the output SINR of the beamformer, Capon proposed the MVDR algorithm:

$$\begin{aligned} &\min_{\boldsymbol{w}} \quad \boldsymbol{w}^H \boldsymbol{R}_{j+n} \boldsymbol{w} \\ &\text{subject to} \quad \boldsymbol{w}^H \boldsymbol{a}(\theta_0) = 1, \end{aligned} \tag{5}$$

where $\boldsymbol{R}_{j+n}$ is the covariance matrix of interference plus noise. In the MVDR beamformer, the output of the desired signal has no distortion and the power of interference plus noise is minimized.

In actual scenarios, the covariance matrix of interference plus noise is difficult to obtain, and $\boldsymbol{R}_{j+n}$ is usually replaced by $\boldsymbol{R}_x$:

$$\boldsymbol{R}_x = \frac{1}{K} \sum_{k=1}^{K} \boldsymbol{x}(k)\, \boldsymbol{x}(k)^H, \tag{6}$$

where K is the snapshot number. The signal self-cancellation phenomenon occurs when a mismatch in the steering vector exists. Signal self-cancellation means that the desired signal is suppressed as interference, and a null appears in the DOA of the desired signal on the beam pattern.

III. PROPOSED BEAMFORMER

To improve the robustness of the beamformer, the factors affecting its performance are analyzed. Assuming that a random point in the space is selected as the coordinate origin, the position of the m-th element in the three-dimensional Cartesian coordinate system can be expressed as

$$\boldsymbol{p}_m = \left[p_{mx} \ , p_{my}, \ p_{mz}\right]^T . \tag{7}$$

When the DOA of the plane wave propagating to the array is $\theta = (\phi, \vartheta)$, the unit vector of the propagation direction can be expressed as

$$\boldsymbol{v}(\theta) = -\left[\sin(\phi)\cos(\vartheta), \sin(\phi)\sin(\theta), \cos(\phi)\right]^T , \tag{8}$$

where ϕ is the elevation angle, and ϑ is the azimuth angle.

The unit response vector of the array, which is also called the array manifold vector, can be expressed as

$$\boldsymbol{a}(\theta) = \left[\exp(-j\boldsymbol{N}^T\boldsymbol{p}_1), \exp(-j\boldsymbol{N}^T\boldsymbol{p}_2), \cdots, \exp(-j\boldsymbol{N}^T\boldsymbol{p}_M)\right]^T , \tag{9}$$

where $\boldsymbol{N} = (2\pi/\lambda)\,\boldsymbol{v}(\theta)$ is the wavenumber.

The response vector of the beamformer to the signal from the direction θ is

$$\begin{aligned} \boldsymbol{b}(\theta) &= \boldsymbol{w}^H\boldsymbol{a}(\theta) \\ &= \boldsymbol{w}^H \exp(-j(2\pi/\lambda)\,\boldsymbol{v}(\theta)^T\boldsymbol{p}), \end{aligned} \tag{10}$$

where $\boldsymbol{w}$ is the weighted vector. Equation (10) indicates that the main factors affecting the response of the beamformer are the weighted vector and the position.

The ideal position of the m-th element of the array is $\bar{\boldsymbol{p}}_m = \left[\bar{p}_{mx}, \bar{p}_{my}, \bar{p}_{mz}\right]^T$ and the actual position is $\boldsymbol{p}_m = \bar{\boldsymbol{p}}_m + \Delta\boldsymbol{p}_m$, where $\Delta\boldsymbol{p}_m = \left[\Delta p_{mx}, \Delta p_{my}, \Delta p_{mz}\right]^T$ is the error vector of the position, $p_{mx} = \bar{p}_{mx} + \Delta p_{mx}$, $p_{my} = \bar{p}_{my} + \Delta p_{my}$, and $p_{mz} = \bar{p}_{mz} + \Delta p_{mz}$. The ideal weighted vector is $\bar{\boldsymbol{w}} = [\bar{w}_1, \bar{w}_2, \cdots, \bar{w}_M]^T$, where the weighted value of the m-th element is $\bar{w}_m^H = \bar{g}_m\exp(j\bar{\varphi}_m)$. That is, the ideal amplitude weighted value is $\bar{g}_m$, and the phase weighted value is $\bar{\varphi}_m$. In practical application scenarios, channel error is inevitable. Therefore, if the channel response is included in the weighted value, then the actual weighted values are different from the ideal weighted values. The actual amplitude and phase weighted values of the m-th element are $g_m = \bar{g}_m(1 + \Delta g_m)$ and $\varphi_m = \bar{\varphi}_m + \Delta\varphi_m$, respectively, where Δg_m and $\Delta\varphi_m$ are the channel amplitude and phase errors, respectively.

Δg_m, $\Delta\varphi_m$, Δp_{mx}, Δp_{my}, and Δp_{mz} are assumed to be zero-mean random variables with a Gaussian distribution and are statistically independent of each other; the variances of Δg_m and $\Delta\varphi_m$ are σ_g^2 and σ_φ^2; and the variance of each component of $\Delta\boldsymbol{p}_m$ is σ_p^2. The ideal beamformer output is

$$\bar{\boldsymbol{b}}(\theta) = \bar{\boldsymbol{w}}^H\bar{\boldsymbol{a}}(\theta) = \sum_{m=1}^{M}\bar{g}_m\exp(j\bar{\varphi}_m - j\boldsymbol{N}^T\bar{\boldsymbol{p}}_m). \tag{11}$$

And the actual beamformer output is

$$\boldsymbol{b}(\theta) = \boldsymbol{w}^H\boldsymbol{a}(\theta) = \sum_{m=1}^{M}g_m\exp(j\varphi_m - j\boldsymbol{N}^T\boldsymbol{p}_m). \tag{12}$$

The mathematical expectation of the square of the actual beamformer output is

$$\begin{aligned} &E\left\{|\boldsymbol{b}(\theta)|^2\right\} \\ &= E\left\{\sum_{i=1}^{M}\sum_{j=1}^{M}g_i\exp\left(j\varphi_i - j\boldsymbol{N}^T\boldsymbol{p}_i\right)g_j\exp\left(j\varphi_j - j\boldsymbol{N}^T\boldsymbol{p}_j\right)\right\} \\ &= \sum_{i=1}^{M}\sum_{j=1}^{M}E\left\{\bar{g}_i(1+\Delta g_i)\,\bar{g}_j(1+\Delta g_j)\right. \\ &\quad\cdot\exp\left(j\left(\bar{\varphi}_i + \Delta\varphi_i - \bar{\varphi}_j - \Delta\varphi_j\right)\right) \\ &\quad\left.\cdot\exp\left(-j\boldsymbol{N}^T\left(\bar{\boldsymbol{p}}_i + \Delta\boldsymbol{p}_i - \bar{\boldsymbol{p}}_j - \Delta\boldsymbol{p}_j\right)\right)\right\}. \end{aligned} \tag{13}$$

α_{ij} and β_{ij} are defined as

$$\alpha_{ij} = E\left\{(1+\Delta g_i)\left(1+\Delta g_j\right)\exp\left(j\left(\Delta\varphi_i - \Delta\varphi_j\right)\right)\right\}, \tag{14}$$

$$\beta_{ij} = E\left\{\exp\left(-j\boldsymbol{N}^T\left(\Delta\boldsymbol{p}_i - \Delta\boldsymbol{p}_j\right)\right)\right\}. \tag{15}$$

Using the assumption of independent Gaussian distribution of random variables, then

$$\alpha_{ij} = \begin{cases}\exp(-\sigma_\varphi^2), & i \neq j \\ 1+\sigma_g^2, & i = j\end{cases}, \tag{16}$$

$$\beta_{ij} = \begin{cases}\exp\left(-\sigma_p^2|\boldsymbol{N}|^2\right) = \exp\left(-\left(\frac{2\pi}{\lambda}\sigma_p\right)^2\right), & i \neq j \\ 1, & i = j.\end{cases} \tag{17}$$

Let $\sigma_\lambda = (2\pi/\lambda)\,\sigma_p$, then (13) can be expressed as

$$\begin{aligned} &E\left\{|\boldsymbol{b}(\theta)|^2\right\} \\ &= \sum_{i=1}^{M}\sum_{\substack{j=1 \\ j\neq i}}^{M}\bar{g}_i\bar{g}_j\exp\left(j\bar{\varphi}_i - j\bar{\varphi}_j\right)\exp\left(-j\boldsymbol{N}^T\left(\bar{\boldsymbol{p}}_i - \bar{\boldsymbol{p}}_j\right)\right) \\ &\quad\cdot\exp\left(-\left(\sigma_\varphi^2 + \sigma_\lambda^2\right)\right) + \sum_{i=1}^{M}\bar{g}_i^2\exp\left(-\left(\sigma_\varphi^2 + \sigma_\lambda^2\right)\right) \\ &\quad + \sum_{i=1}^{M}\bar{g}_i^2\left(1+\sigma_g^2\right) - \sum_{i=1}^{M}\bar{g}_i^2\exp\left(-\left(\sigma_\varphi^2 + \sigma_\lambda^2\right)\right) \\ &= \left|\bar{\boldsymbol{b}}(\theta)\right|^2\exp\left(-\left(\sigma_\varphi^2 + \sigma_\lambda^2\right)\right) \\ &\quad + \sum_{m=1}^{M}\bar{g}_m^2\left(1+\sigma_g^2 - \exp\left(-\left(\sigma_\varphi^2 + \sigma_\lambda^2\right)\right)\right). \end{aligned} \tag{18}$$

Equation (18) shows that the influence of the small errors in element position, channel amplitude, and channel phase on the beamformer output reduces with the decrease of the weighted vector norm.

To improve the robustness of the beamformer, the idea of minimizing each element in the weighted vector is considered. Fortunately, when the l_2-norm of the vector is minimized, the value of each element in the vector becomes very small. According to this characteristic, the weighted vector

norm is added to the objective function of the MVDR model, and the following optimization problem is proposed:

$$\begin{aligned} \min_{\boldsymbol{w}} \quad & \boldsymbol{w}^H \boldsymbol{R}_x \boldsymbol{w} + \gamma \|\boldsymbol{w}\| \\ \text{subject to} \quad & \boldsymbol{w}^H \boldsymbol{a}(\theta_0) = 1, \end{aligned} \tag{19}$$

where $\|\cdot\|$ denotes the l_2-norm, and $\gamma \in (0, +\infty)$ is the regularization coefficient.

The equality constraint function in optimization problem (19) transforms $\boldsymbol{w}$ from M-dimensional space to one-dimensional space, so the equality constraint is affine. The objective function is defined as

$$F(\boldsymbol{w}) \triangleq \boldsymbol{w}^H \boldsymbol{R} \boldsymbol{w} + \gamma \|\boldsymbol{w}\|. \tag{20}$$

Variable $\beta \in [0, 1]$ is introduced. Then, inequality $F(\beta \boldsymbol{w}_1 + (1-\beta)\boldsymbol{w}_2) \leq \beta F(\boldsymbol{w}_1) + (1-\beta) F(\boldsymbol{w}_2)$ holds, where $\boldsymbol{w}_1$ and $\boldsymbol{w}_2$ are any two vectors in the feasible region. This relationship proves that the objective function $F(\boldsymbol{w})$ is convex. Given that the equality constraint is affine, the proposed optimization model (19) is proved to be a convex optimization problem.

The objective function of (19) reveals that the balance between the output power and the robustness can be achieved by selecting an appropriate regularization coefficient γ. Inspired by the L-curve method [28], some data with a logarithmic interval distribution in a certain range are taken as values of γ. The relationship between the output power and the weighted vector norm can be obtained by solving the optimization problem (19) with different values of γ. The curve of the weighted vector norm changing with the output power of the array is L-shaped. The γ value corresponding to the corner of the L-curve is the optimal value of γ for balancing the output power and the robustness.

IV. COMPUTER SIMULATIONS

Computer simulations were conducted to demonstrate the method of finding the optimal regularization coefficient and verify the robustness improvement of the WVNR algorithm compared with the MVDR algorithm.

An irregular arc array with 62 elements was used. All elements are omnidirectional, and the position of the elements in the array is shown in Figure 1.

In the following simulations, the desired signal and interferences are plane waves propagating to the array, the noise in space is Gaussian additive white noise, and the speed of propagation is 1500 m/s. In all simulations, the elevation angles of the assumed and actual steering vectors are both 90°. Thus, only the azimuth angle of the steering vector is considered. For the convenience of expression, the azimuth angle is replaced by the angle. In the beam pattern simulations, the angle of the assumed steering vector is 0°; the DOAs of interferences are −25°, 25°, and 65°; the SNR is 10 dB; and the interference to noise ratio (INR) is 30 dB. Computer simulations are carried out under different conditions: (a) the mismatch range of the steering vector is [−2°, 2°]; (b) the mismatch range of the steering vector is [−5°, 5°].

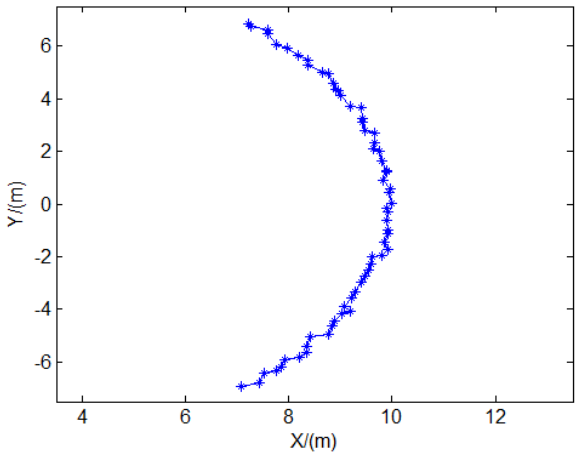

FIGURE 1. Element position of the irregular arc array.

A. REGULARIZATION COEDDICIENT

To find the appropriate regularization coefficient γ, 50 data with a logarithmic interval distribution in the range of $[10^{-1}, 10^{4}]$ are taken as the values of γ. The L-curve of the weighted vector norm to the output power is shown in Figure 2, the output power versus the regularization coefficient is presented in Figure 3.

In Figures 2 and 3, (a) and (b) correspond to the case where the maximum absolute value of the steering vector mismatch is 2° and 5°, respectively. Figures 2 and 3 indicate that the method to find the appropriate regularization coefficient can be divided into the following two steps.

1. According to Figure 2, the fitting curve of the log-log scaled L-curve can be obtained by the fitting cubic spline method. Then, the curvature of the fitting curve can be calculated. The maximum curvature of the fitting curve corresponds to the corner of the L-curve for which the corresponding output power can be found.

2. Figure 3 and the output power corresponding to the maximum curvature reveal the value of the regularization coefficient corresponding to the corner of the L-curve. This value can ensure that the beamformer is robust within the mismatch range of the steering vector.

The comparison of Figures 2(a) and 2(b) reveals that the position of the turning point of the L-curve varies with the mismatch range of the steering vector. Furthermore, considering the corresponding relationship between the regularization coefficient and the output power in Figure 3, the appropriate value of the regularization coefficient γ varies with the mismatch range of steering vector.

In the following simulations, the value of regularization coefficient γ is 559 when the mismatch range of the steering vector is [−2°, 2°] and 576 when the mismatch range is [−5°, 5°].

B. BEAM PATTERN

The beam patterns of CBF, MVDR, and WVNR are compared in Figure 4. In Figures 4(a) and 4(b), the angle of the actual steering vector is 2° and 5°, respectively.

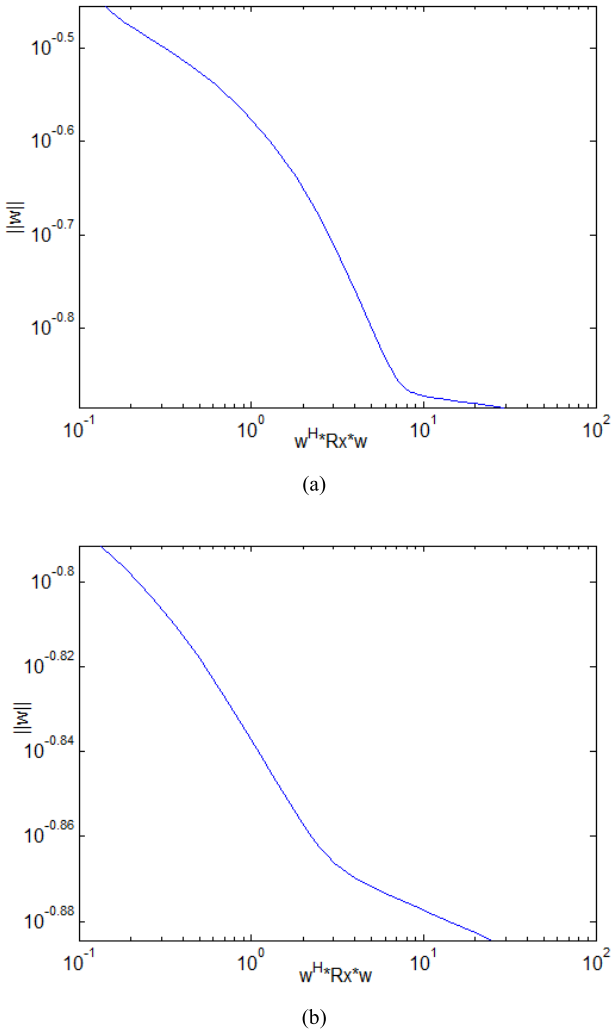

FIGURE 2. Output power versus weighted vector norm. The mismatch range of the assumed steering vector is (a) [−2°, 2°]; (b) [−5°, 5°].

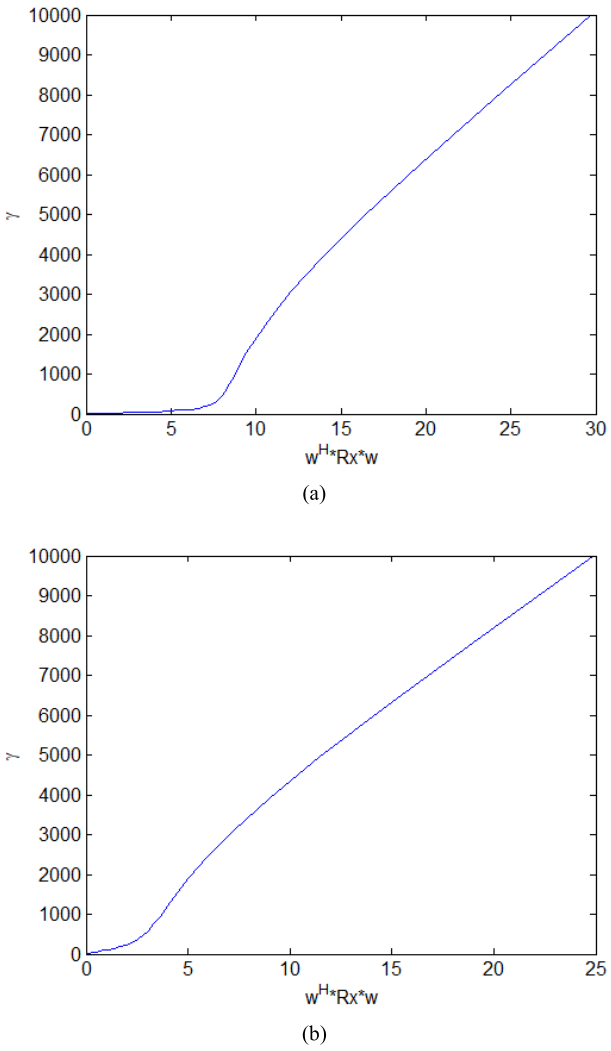

FIGURE 3. Output power versus regularization coefficient. The mismatch range of the assumed steering vector is (a) [−2°, 2°]; (b) [−5°, 5°].

In Figures 4(a) and 4(b), WVNR and CBF obtain the maximum value in the 0° direction, and the nulls in the −25°, 25°, and 65° directions are formed by WVNR and MVDR. In Figures 4(a) and 4(b), a null is formed by MVDR in the 2° direction and 5° direction, respectively.

In Figure 4, when the regularization coefficient is set to an appropriate value, both WVNR and CBF can ensure the strongest signal amplification ability in the direction of the assumed steering vector. The interference suppression ability of WVNR is weaker than that of MVDR but stronger than that of CBF. When the steering vector is mismatched, MVDR mistakenly takes the desired signal as interference and suppresses it. Figure 4 shows that the order of interference suppression ability from strong to weak is MVDR, WVNR, and CBF.

C. SINR VERSUS SNAPSHOT NUMBER

The number of repetitions is 500. The average value of the output SINR is recorded, and the variation of the output SINR with the number of snapshots is shown in Figure 5. In Figures 5(a) and 5(b), the angle of the actual steering vector is 2° and 5° respectively.

In Figure 5(a), the output SINR of CBF is always -12.25 dB; in Figure 5(b), the output SINR of CBF is always -15.72 dB. The output SINR of WVNR in Figure 5(a) increased rapidly from 16.71 dB to 16.82 dB and remained unchanged with the increase of the number of snapshots, while the output SINR of WVNR in Figure 5(b) increased quickly from 11.97 dB to 12.07 dB and then remained the same. In Figures 5(a) and 5(b), the output SINR of MVDR decreased as the number of snapshots increased. In Figure 5(a), the output SINR of MVDR decreased from -10.38 dB to -18.44 dB; in Figure 5(b), the output SINR of MVDR decreased from -10.87 dB to -24.42 dB.

Figure 5 shows that the output SINR of CBF remained unchanged with the increase in the number of snapshots, while the output SINR of WVNR only increased by 0.1 dB. In Figures 5(a) and 5(b), the changes in the output SINR of

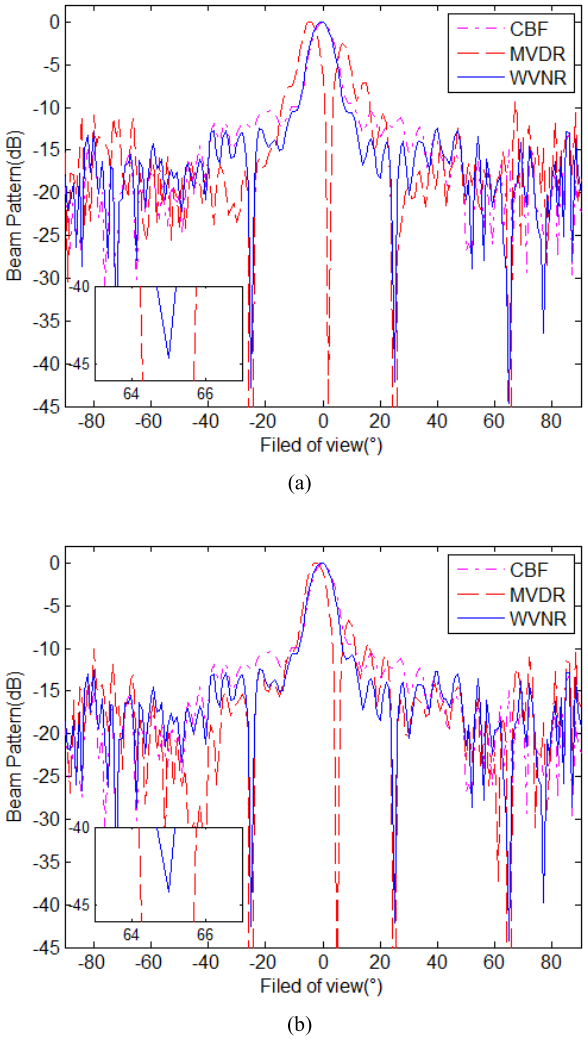

FIGURE 4. Beam pattern. The angle of the actual steering vector is (a) 2°; (b) 5°.

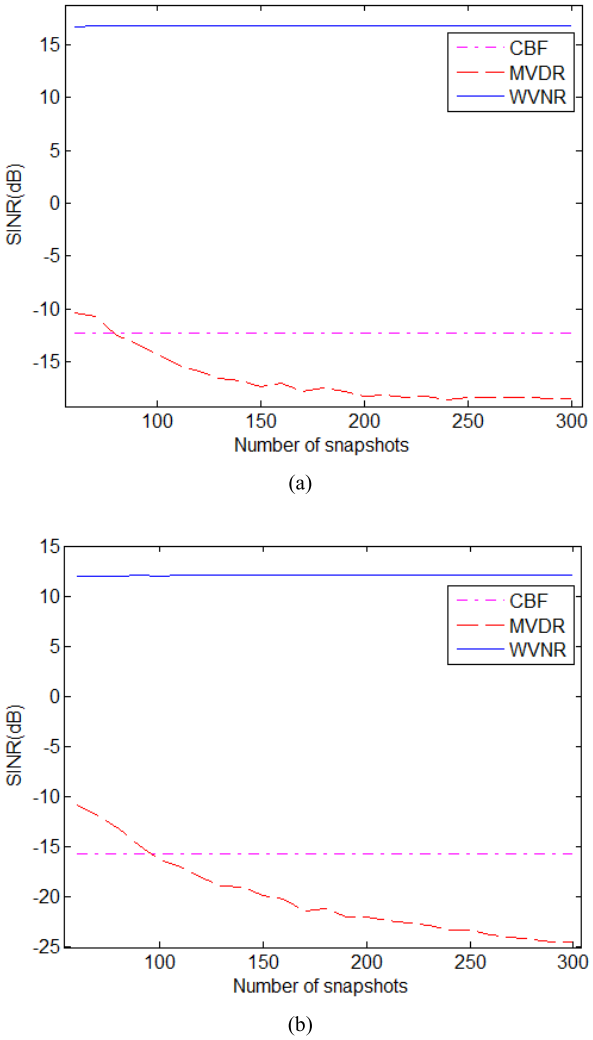

FIGURE 5. SINR versus number of snapshots. The number of repetitions is 500, the angle of the actual steering vector is (a) 2°; (b) 5°.

MVDR are 8.06 dB and 13.55 dB, respectively. Figure 5 illustrates that the order of robustness to the snapshot number from strong to weak is CBF, WVNR, and MVDR.

D. SINR VERSUS MISMATCH

The number of snapshots is 150, the number of repetitions is 500. The average value of the output SINR is recorded, and the curves of SINR versus the mismatch of the steering vector are shown in Figure 6. In Figure 6(a), the mismatch of the steering vector changes from $-2°$ to $2°$; in Figure 6(b), the mismatch of the steering vector changes from $-5°$ to $5°$.

Figure 6(a) shows that the output SINRs of CBF, MVDR, and WVNR decreased from -11.64 dB to -12.25 dB, 3.74 dB to -17.04 dB, and 17.68 dB to 16.73 dB, respectively, with the increase in the absolute value of the steering vector mismatch from 0° to 2°. Figure 6(b) indicates that the output SINRs of CBF, MVDR, and WVNR decreased from -11.64 dB to -15.77 dB, 3.74 dB to -20.19 dB, and 17.48 dB to 11.99 dB, respectively, with the increase in the absolute value of the steering vector mismatch from 0° to 5°.

Figure 6(a) shows that the output SINRs of CBF, MVDR, and WVNR decreased by 0.61 dB, 20.78 dB, and 0.95 dB, respectively, as the absolute value of the steering vector mismatch increased by 2°. Figure 6(b) indicates that the output SINRs of CBF, MVDR, and WVNR decreased by 4.13 dB, 23.93 dB, and 5.49 dB, respectively, as the absolute value of the steering vector mismatch increased by 5°. Figure 6 implies that the order of robustness to the mismatch of the steering vector from strong to weak is CBF, WVNR, and MVDR. Furthermore, the output SINR of WVNR in Figure 6(a) is always slightly higher than that in Figure 6(b) when the steering vector mismatch is the same. This phenomenon indicates that the output SINR of the WVNR beamformer increases gradually with the narrowing of the mismatch range of the steering vector.

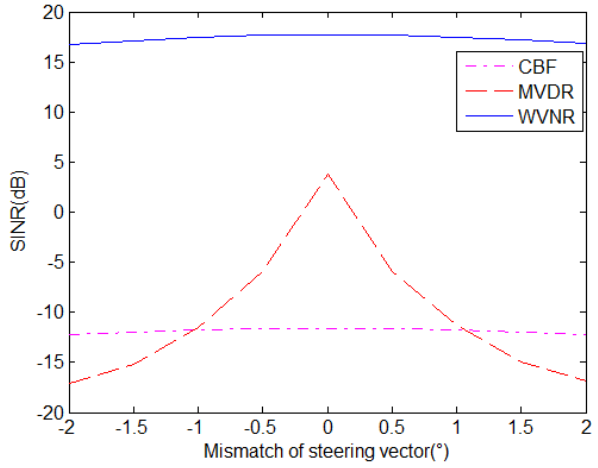

(a)

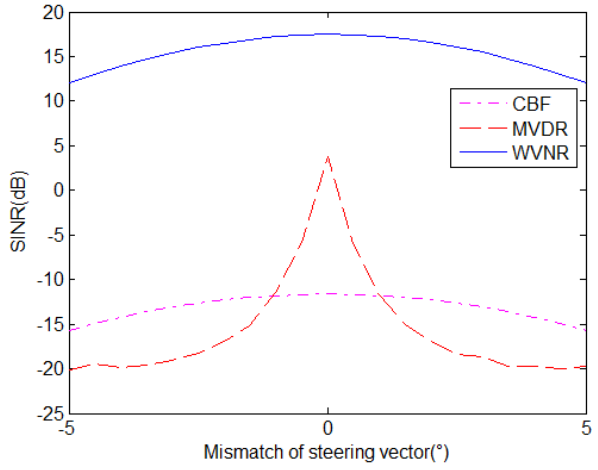

(b)

FIGURE 6. SINR versus mismatch. The number of snapshots is 150, the number of repetitions is 500, the mismatch range of the assumed steering vector is (a) [−2°, 2°]; (b) [−5°, 5°].

V. CONCLUSION

In this study, the WVNR beamforming method is proposed. In the WVNR beamforming method, the regularization term is used to directly control the robustness of the beamformer, and the regularization coefficient is used to adjust the balance between the output power and the robustness. The main lobe shape, the ability to suppress interference, and the robustness to the snapshot number are simultaneously considered as reflected in the following aspects: (1) the shape of the main lobe remains unchanged; (2) null is formed in the DOA of interference; (3) the impact of the change in snapshot number on performance. When the steering vectors do not match or the snapshot number is insufficient, the serious degradation of the performance of the MVDR beamformer is effectively solved by the WVNR method. The WVNR algorithm can ensure that the spatial resolution remains unchanged, and reduce the influence of the snapshot number on performance. However, the ability to suppress interference inevitably decreases as reflected by the shallow depth of the null in the DOA of interference. Consequently, the beamformer gains the above advantages while slightly sacrificing its interference suppression ability. Therefore, the WVNR method is suitable in cases of steering vector mismatch or insufficient snapshot number. In future work, the influence of the $l_{1/\infty}$-norm of the weighted vector on robustness can be discussed.

REFERENCES

[1] M.-M. Zhao, A. Liu, and R. Zhang, "Outage-constrained robust beamforming for intelligent reflecting surface aided wireless communication," *IEEE Trans. Signal Process.*, vol. 69, pp. 1301–1316, 2021, doi: 10.1109/tsp.2021.3056899.

[2] F. Paisana, G. A. Ropokis, N. Marchetti, and L. A. DaSilva, "Cognitive beamforming in radar bands," *IEEE Trans. Commun.*, vol. 66, no. 8, pp. 3623–3637, Aug. 2018, doi: 10.1109/tcomm.2018.2817543.

[3] Y. Hao, N. Zou, and G. L. Liang, "Robust capon beamforming against steering vector error dominated by large direction-of-arrival mismatch for passive sonar," *J. Marine Sci. Eng.*, vol. 7, no. 3, p. 16, Mar. 2019, doi: 10.3390/jmse7030080.

[4] M. Mozaffarzadeh, M. Sadeghi, A. Mahloojifar, and M. Orooji, "Double-stage delay multiply and sum beamforming algorithm applied to ultrasound medical imaging," *Ultrasound Med. Biol.*, vol. 44, no. 3, pp. 677–686, Mar. 2018, doi: 10.1016/j.ultrasmedbiO.2017.10.020.

[5] P. Chiariotti, G. Battista, M. Ettorre, and P. Castellini, "Average acoustic beamforming in car cabins: An automatic system for acoustic mapping over 3D surfaces," *Appl. Acoust.*, vol. 129, pp. 47–63, Jan. 2018, doi: 10.1016/j.apacoust.2017.07.009.

[6] O. A. Iupikov, M. V. Ivashina, N. Skou, C. Cappellin, K. Pontoppidan, and C. G. M. van 't Klooster, "Multibeam focal plane arrays with digital beamforming for high precision space-borne ocean remote sensing," *IEEE Trans. Antennas Propag.*, vol. 66, no. 2, pp. 737–748, Feb. 2018, doi: 10.1109/tap.2017.2763174.

[7] J. Capon, "High-resolution frequency-wavenumber spectrum analysis," *Proc. IEEE*, vol. 57, no. 8, pp. 1408–1418, Aug. 1969, doi: 10.1109/proc.1969.7278.

[8] J. Liu, A. B. Gershman, Z.-Q. Luo, and K. Max Wong, "Adaptive beamforming with sidelobe control: A second-order cone programming approach," *IEEE Signal Process. Lett.*, vol. 10, no. 11, pp. 331–334, Nov. 2003, doi: 10.1109/LSP.2003.817852.

[9] M. Wax and Y. Anu, "Performance analysis of the minimum variance beamformer in the presence of steering vector errors," *IEEE Trans. Signal Process.*, vol. 44, no. 4, pp. 938–947, Apr. 1996, doi: 10.1109/78.492546.

[10] B. D. Carlson, "Covariance matrix estimation errors and diagonal loading in adaptive arrays," *IEEE Trans. Aerosp. Electron. Syst.*, vol. AES-24, no. 4, pp. 397–401, Jul. 1988, doi: 10.1109/7.7181.

[11] O. Besson and F. Vincent, "Performance analysis of beamformers using generalized loading of the covariance matrix in the presence of random steering vector errors," *IEEE Trans. Signal Process.*, vol. 53, no. 2, pp. 452–459, Feb. 2005, doi: 10.1109/TSP.2004.840777.

[12] L. Chang and C.-C. Yeh, "Performance of DMI and eigenspace-based beamformers," *IEEE Trans. Antennas Propag.*, vol. 40, no. 11, pp. 1336–1347, 1992, doi: 10.1109/8.202711.

[13] D. D. Feldman and L. J. Griffiths, "A projection approach for robust adaptive beamforming," *IEEE Trans. Signal Process.*, vol. 42, no. 4, pp. 867–876, Apr. 1994, doi: 10.1109/78.285650.

[14] Y. Xiao, J. Yin, H. Qi, H. Yin, and G. Hua, "MVDR algorithm based on estimated diagonal loading for beamforming," *Math. Problems Eng.*, vol. 2017, pp. 1–7, Jan. 2017, doi: 10.1155/2017/7904356.

[15] W. Li, Y. Zhao, Q. Ye, and B. Yang, "Adaptive antenna null broadening beamforming against array calibration error based on adaptive variable diagonal loading," *Int. J. Antennas Propag.*, vol. 2017, pp. 1–9, Oct. 2017, doi: 10.1155/2017/3265236.

[16] Y. Ke, C. Zheng, R. Peng, and X. Li, "Robust adaptive beamforming using noise reduction preprocessing-based fully automatic diagonal loading and steering vector estimation," *IEEE Access*, vol. 5, pp. 12974–12987, 2017, doi: 10.1109/access.2017.2725450.

[17] J. Wang, W. Zhang, and W. Liu, "Minimum sensitivity based robust beamforming with eigenspace decomposition," *Multidimensional Syst. Signal Process.*, vol. 29, no. 2, pp. 687–701, Apr. 2018, doi: 10.1007/s11045-016-0424-1.

[18] C. Wang, J. Tang, and B. Yang, "Fast and convenient implementation of iterative eigenspace-based beamforming," *Electron. Lett.*, vol. 51, no. 9, pp. 720–722, Apr. 2015, doi: 10.1049/el.2015.0131.
[19] L. Rebollo-Neira and A. Plastino, "Sparse representation of gravitational sound," *J. Sound Vib.*, vol. 417, pp. 306–314, Mar. 2018, doi: 10.1016/j.jsv.2017.12.007.
[20] M. Abavisani and V. M. Patel, "Deep sparse representation-based classification," *IEEE Signal Process. Lett.*, vol. 26, no. 6, pp. 948–952, Jun. 2019, doi: 10.1109/lsp.2019.2913022.
[21] X. Yang, L. Jian, B. Yan, K. Liu, L. Zhang, and Y. Liu, "A sparse representation based pansharpening method," *Future Gener. Comput. Syst.*, vol. 88, pp. 385–399, Nov. 2018, doi: 10.1016/j.future.2018.04.096.
[22] Y. L. Huang, Y. G. Xu, S. L. Shi, K. Zhao, and Z. W. Liu, "Sparse representation approaches to parameter estimation of completely polarized wideband signals," *Signal Process.*, vol. 171, p. 15, Jun. 2020, doi: 10.1016/j.sigpro.2020.107521.
[23] Y. Zhang, B. P. Ng, and Q. Wan, "Sidelobe suppression for adaptive beamforming with sparse constraint on beam pattern," *Electron. Lett.*, vol. 44, no. 10, p. 615, 2008, doi: 10.1049/el:20080415.
[24] L. Zhen, S. Chao, L. Xiong-Hou, and G. Qi-Li, "Robust capon beamforming with weighted sparse constraint," *Acta Phys. Sinica*, vol. 65, no. 10, 2016, Art. no. 104303, doi: 10.7498/aps.65.104303.
[25] L. Yang, Y. Yang, and J. Yang, "Robust adaptive beamforming for uniform linear arrays with sensor gain and phase uncertainties," *IEEE Access*, vol. 7, pp. 2677–2685, 2019, doi: 10.1109/ACCESS.2018.2886405.
[26] X. Ren, Y. Wang, T. Guo, and Q. Wang, "Robust adaptive beamforming using support vector machines," *IEEE Access*, vol. 8, pp. 137955–137965, 2020, doi: 10.1109/access.2020.3009993.
[27] L. Yang, Y. Yang, G. Liao, and X. Guo, "Joint calibration of array shape and sensor gain/phase for highly deformed arrays using wideband signals," *Signal Process.*, vol. 165, pp. 222–232, Dec. 2019, doi: 10.1016/j.sigpro.2019.07.011.
[28] P. C. Hansen and D. P. O'Leary, "The use of the L-curve in the regularization of discrete ill-posed problems," *SIAM J. Sci. Comput.*, vol. 14, no. 6, pp. 1487–1503, Nov. 1993, doi: 10.1137/0914086.

XIAOYING REN received the B.S. degree in electronic information engineering and the M.S. degree in electronic and communication engineering from Xi'an Shiyou University, Xi'an, China, in 2012 and 2015, respectively. She is currently pursuing the Ph.D. degree in underwater acoustics engineering at Northwestern Polytechnical University, Xi'an. She attended the 2018 OCEANS—MTS/IEEE Kobe Techno Oceans (OTO) International Conference and presented her research results orally at the conference. Her research interests include array signal processing, artificial intelligence algorithm, and compressive sensing.

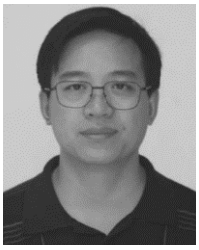

YINGMIN WANG (Member, IEEE) received the B.S. degree in electronic engineering, the M.S. degree in underwater acoustics, and the Ph.D. degree in weapon system and application from Northwestern Polytechnical University (NPU), Xi'an, China, in 1983, 1988, and 2002, respectively.

Since 1983, he has been with the College of Marine Engineering, NPU, where he is currently a Professor and a Doctoral Supervisor. From 1994 to 1995, he was a Research Fellow with the Sonar and Radar Group, School of Electronic, Electrical and Computer Engineering, University of Birmingham, Birmingham, U.K., where he developed simulated annealing algorithms for underwater acoustic data processing. From 2000 to 2001, he was a Visiting Research Fellow with the Department of Electrical and Computer Engineering, University of Minnesota, Twin Cities, Minneapolis, MN, USA, where he worked on problems on the blind source separation related to sound propagation and scattering. His current research interests include genetic algorithms, optimization theories, sonar array processing, and underwater acoustic systems. He is also a member of the Acoustical Society of America.

LICHEN ZHANG born in Tangshan, Hebei, China, in 1986. He received the B.S. degree in information countermeasure technology from Northwestern Polytechnic University, in 2009, the M.S. and Ph.D. degrees in underwater acoustic engineering from Northwestern Polytechnic University, in 2012 and 2018, respectively.

He has been an Engineer with the Systems Engineering Research Institute, since 2017. His research interests include array signal processing, vector hydrophone technology, and underwater acoustic target characteristics.

QI WANG was born in Weinan, Shaanxi, China, in 1983. He received the B.S. degree in information countermeasure technology and the M.S. and Ph.D. degrees in underwater acoustic engineering from Northwestern Polytechnical University, Xi'an, China, in 2007, 2010, and 2015, respectively.

From 2016 to 2017, he carried out postdoctoral work in the School of Marine Science and Technology, Northwestern Polytechnical University. Since 2017, he has been carried out engineering research in the Xi'an University of technology. Since 2019, he has the title of the Deputy Researcher. His current research interests include underwater acoustic signal processing, genetic algorithms, optimization theories, and artificial intelligence algorithm.